

# **Solvent effects on the nonlinear optical response of a potentiometric biological imaging dye**

Haowen Li, Guilin Mao and Kenneth D. Singer

*Case Western Reserve University, Department of Physics, Cleveland, OH 44106-7079*

Zhikuan Lu, Ryan Weber, Robert J. Twieg

*Kent State University, Department of Chemistry, Kent, OH 44242*

## **Abstract**

In order to understand the electronic mechanisms for the electric-field sensitive second harmonic response of di-8-ANEPPS in biological membranes, we have measured its nonlinear optical hyperpolarizability using a combination of Hyper-Rayleigh scattering (HRS) and linear optical properties in solvent environments of various polarity. Changes in the first hyperpolarizabilities are discussed by modeling experimental inputs from the solvatochromic effect in linear absorption and appropriate dispersion relations near the two-photon resonance. We find that both frequency dependent and frequency independent effects make significant contributions to the response, and the strongest response is on the low energy side of the two-photon resonance, while the weakest response is on the high energy side of the two-photon resonance.

OCIS Codes: 190.4710, 170.3880, 300.6420

## Introduction

First developed by Loew and colleagues,<sup>1,2</sup> the fluorescent dye di-8-ANEPPS (4-(2-[6-(dioctylamino)-2-naphthalenyl]ethenyl)-1-(3-sulfopropyl) pyridinium inner salt) as shown in Figure (1), consists of a quaternized pyridinium electron acceptor moiety linked by a  $\pi$ -bond to an amino substituted naphthalene electron donor.<sup>3</sup> It has been extensively used as a potential sensitive dye to probe, via linear and nonlinear optics, the electrical environment in biological membranes due to changes in its optical properties as a function of the local electric field. Considerable work has been done in order to determine the mechanism of the nonlinear optical sensitivity and the mode of optimum use of ANEPPS and other probe dyes.<sup>4-11</sup> Studies in Loew's laboratory have shown that electrochromism (Stark shift) is an important component of the dye response to potential sensitivity.<sup>9-11</sup> The chromophore's electron density is concentrated in the amino-naphthalene ring in the ground state and shifts to the pyridinium ring in the excited state; this charge-shift couples with an electric field within a cell membrane, resulting in electrochromism.

It has been found that probing membrane potential using second harmonic generation is superior to fluorescence modalities because of the requirement for noncentrosymmetric media leading to high membrane specificity and contrast, low background, and high spatial resolution in deep scattering specimens.<sup>12-15</sup> Recently, the molecular orientation of di-8-ANEPPS and similar dyes in black lipid membranes (BLM)<sup>4</sup> and giant unilamellar vesicles (GUV)<sup>5, 6</sup> and its effects on potential sensitivity have also been discussed using second harmonic generation. The potential response may

arise purely from electrically induced changes in the molecular electronic hyperpolarizability  $\beta$ , or by a combination of this and molecular reorientation by the external electric field. Several papers have theoretically and experimentally discussed the two-photon fluorescence or second harmonic sensitivity of ANEPPS and similar potential dyes.<sup>16-20</sup> In particular, Pons and Mertz<sup>16</sup> recently examined theoretically the Stark shift mechanism near the two-photon resonance.

In this paper, we seek to examine the purely electronic mechanism for electric-field dependent second harmonic generation using solvent dependent optical properties. To do so, we have carried out linear and nonlinear optical studies of the di-8-ANEPPS dye in liquid solution. It is well-known that solvent polarity is closely related to the local electric field surrounding a dissolved molecule.<sup>21</sup> We use polarity-dependent solvent studies of linear absorption and hyper-Rayleigh scattering in solution to probe the spectral dependence of the sensitivity to the local environment. We also model this sensitivity using a two-level model by including the spectral shift, changes in transition moment, excited and ground state dipole moment difference, and spectral width as the local electric field (solvent polarity) is varied. We model the relationship between first hyperpolarizability,  $\beta$ , and linear absorption spectrum as a function of solvent polarity and, by inference, local electric field. We find good agreement between the model and the measurements. Our work suggests a cuvette-based linear optical technique for estimating the sensitivity response of potentiometric dye candidates.

We note that while di-8-ANNEPS is not the only second-harmonic potentiometric dye currently in use, we have chosen to study it here because of the large body of literature on it, and because of its good solubility in a variety of organic solvents. We

believe that the results and conclusions found here are more generally applicable and we plan further studies on other dyes to verify this.

## Methods and Theory

Hyper-Rayleigh scattering (HRS) has been established as a powerful tool for measuring the first-order electronic hyperpolarizability  $\beta$ .<sup>22, 23</sup> It involves illumination of a sample in isotropic solution at frequency  $\omega$  and detection of the scattered incoherent second-harmonic photons at  $2\omega$ . Since HRS does not involve the use of an external static electric field, it can measure both polar and non-polar as well as charged and uncharged materials,<sup>24</sup> making it particularly appropriate for measurement of di-8-ANEPPS.

In order to obtain the hyperpolarizability  $\beta$  value for di-8-ANEPPS, an external referencing method is used. A well-studied molecule, para-nitroaniline (pNA) is used as the reference compound. The HRS intensity is measured as a function of concentration for the di-8-ANEPPS and pNA under identical experimental conditions. Due to the incoherent nature of the HRS process, for a two component solvent-solute system, the HRS intensity can be written as a sum of the intensities from the solvent and the dye molecules<sup>25</sup>:  $I(2\omega) = G(N_{solvent} \langle \beta_{solvent}^2 \rangle + N_{solute} \langle \beta_{solute}^2 \rangle) I_0^2 e^{-CN_{solute}}$  where G is a geometrical, local field and instrumental prefactor. The quantities  $N_{solvent}$  and  $N_{solute}$  are the number densities of the solvent and solute, respectively, and  $\langle \beta_{solvent}^2 \rangle$  and  $\langle \beta_{solute}^2 \rangle$  are the molecular hyperpolarizabilities squared and averaged over orientation fluctuations. The quantity  $I_0$  is the intensity of the fundamental laser, and  $e^{-CN_{solute}}$  is the Beer–Lambert Law to account for the absorption of the HRS if the scattered light wavelength lies in the absorption band of the dye solution. If we use A and B to substitute

the variables in the above equation we obtain:  $A = GI_0^2 N_{solvent} \langle \beta_{solvent}^2 \rangle$ ,  $B = GI_0^2 \langle \beta_{solute}^2 \rangle$ , Thus:  $I_{2\omega} = (A + BN_{solute})e^{-CN_{solute}}$ . By varying the concentration of solute, in the limit of low concentration, the number density of the solvent  $N_{solvent}$  does not vary appreciably so that we can obtain the concentration dependence by a fit of the experimental data with intercept A, linear factor B, and extinction factor C. By comparing the data for pNA and the dye, we obtain:  $\frac{B_{pNA}}{B_{dye}} = \frac{\langle \beta_{pNA}^2 \rangle}{\langle \beta_{dye}^2 \rangle}$ . With the knowledge of  $\beta_{pNA}$ , the  $\beta_{dye}$  can be easily calculated.

Since the di-8-ANEPPS chromophore is an asymmetric conjugated  $\pi$ -electron system possessing a large hyperpolarizability in the charge-transfer direction, it might be described using a one-dimensional, two-level model (TLM), originally developed by Oudar and Chemla:<sup>26</sup>

$$\beta = \frac{3\Delta\mu \cdot |\mu_{ge}|^2}{\hbar^2 \omega_0^2} \frac{\omega_0^4}{(\omega_0^2 - \omega^2)(\omega_0^2 - 4\omega^2)} \quad (1)$$

Here  $\hbar$  is Planck's constant,  $\omega_0$  the resonance frequency,  $\Delta\mu = \mu_e - \mu_g$  the difference in the dipole moment between the excited (e) and ground (g) states, and  $\mu_{ge}$  the transition dipole moment. As we show later, depolarization measurements do indeed suggest that the chromophore is quasi-one-dimensional and, therefore, makes the two-level model reasonably descriptive. Since we are carrying out measurements near the two-photon resonance, an appropriate model for damping must be included to properly describe the dispersion. In general, this implies that

$$\beta = \beta(2\omega, \omega_0, \Delta\mu, \mu_{ge}, \gamma) \quad (2)$$

where the functional form is that which appropriately describes the broadening mechanism depending on the broadening factor,  $\gamma$ .

The second harmonic sensitivity to local field is actually described by the EFISH, or electric-field-induced second harmonic coefficient, a third order nonlinear optical response function. However, direct EFISH measurements in solution or even in membranes will yield both electronic (the quantity wanted here) *and* orientational responses. In solution, the EFISH orientational response is much larger.

The electrochromic and solvatochromic response, that is the change in intensity due to the change in the local field, for optical second harmonic generation can be estimated from  $\frac{dI_{2\omega}}{dE_{loc}} = \frac{d}{dE_{loc}} \left( |\chi^{(2)}| E^2 \right)^2$ , where  $E_{loc}$  is the local electric field that is, in the case considered here, related to solvent polarity. The nonlinear optical susceptibility  $\chi^{(2)}$  is proportional to the hyperpolarizability  $\beta$  so we can calculate the relative changes of the amplitude of  $\beta$  as a function of local electric field, or the sensitivity as:

$$\frac{1}{|\beta|^2} \frac{d|\beta|^2}{dE_{loc}} = \frac{2}{|\beta|} \frac{d|\beta|}{dE_{loc}}. E_{loc} \text{ can be expressed using } F, \text{ a polarity indicator in solvents,}$$

which is a function of solvent dielectric constant and refractive index:<sup>27</sup>

$$F(n, \varepsilon) = \frac{1}{\varepsilon_i} \left( \frac{\varepsilon_i - n^2}{\varepsilon_i + 2n^2} - \frac{\varepsilon_i - \varepsilon}{\varepsilon_i + 2\varepsilon} \right) \text{ and } \varepsilon_i = 2, \text{ an empirical parameter, is taken as the}$$

intermediate dielectric constant.

The sensitivity, or relative change in the amplitude of  $\beta$  as a function of polarity (local electric field) can be written as:

$$\begin{aligned}
\frac{1}{|\beta|} \frac{d|\beta|}{dF} = & \frac{1}{|\beta|} \frac{\partial \Delta\mu}{\partial F} \frac{\partial |\beta|}{\partial \Delta\mu} \Bigg|_{\bar{\mu}_{ge}, \bar{\omega}_0, \bar{\gamma}} + \frac{1}{|\beta|} \frac{\partial \mu_{ge}}{\partial F} \frac{\partial |\beta|}{\partial \mu_{ge}} \Bigg|_{\Delta\bar{\mu}, \bar{\omega}_0, \bar{\gamma}} \\
& + \frac{1}{|\beta|} \frac{\partial \omega_0}{\partial F} \frac{\partial |\beta|}{\partial \omega_0} \Bigg|_{\Delta\bar{\mu}, \bar{\mu}_{ge}, \bar{\gamma}} + \frac{1}{|\beta|} \frac{\partial \gamma}{\partial F} \frac{\partial |\beta|}{\partial \gamma} \Bigg|_{\Delta\bar{\mu}, \bar{\mu}_{ge}, \bar{\omega}_0}
\end{aligned} \tag{3}$$

where barred denote mean values used to numerically evaluate the partial derivatives of the analytical expression for  $|\beta|$ . Equation (3) provides a model for understanding the mechanism for the electric field dependent second harmonic response (electronic contribution to the electric field induced second harmonic generation, EFISH). We will measure the left-hand side of Equation (3) directly using hyper-Rayleigh scattering in solutions of various  $F$ . We will compare these HRS measurements to the right-hand side of the equation using solvatochromic measurements of linear absorption to determine the

F dependence of  $\mu_{ge}$ ,  $\omega_0$ , and  $\gamma$ , i.e.  $\frac{\partial \mu_{ge}}{\partial F}$ ,  $\frac{\partial \omega_0}{\partial F}$ ,  $\frac{\partial \gamma}{\partial F}$ . The F dependence of  $\Delta\mu$ ,  $\frac{\partial \Delta\mu}{\partial F}$ , will

be determined from hyper-Rayleigh measurements and an appropriate model for  $\beta$ . The

factors on the right of the form  $\frac{1}{|\beta|} \frac{\partial |\beta|}{\partial u} \Bigg|_{\bar{v}, \bar{w}, \bar{x}}$  require an analytical model for dispersion of

$\beta$  near the two-photon resonance as well as average values for parameters held fixed.

Models for the dispersion of  $\beta$  near the two-photon resonance have been widely discussed in the literature. This discussion basically centers on the appropriate description of broadening near the resonance. The original model is based on a simple Classical Damped Harmonic Oscillator (CDHO) introduced as  $\omega_0 = \omega_0 - i\gamma$ , where  $\beta$  can be written as<sup>28</sup>:

$$\beta = \frac{\Delta\mu \cdot |\mu_{ge}|^2}{\hbar^2} \left\{ \frac{1}{(\omega_0 + i\gamma + 2\omega)(\omega_0 + i\gamma + \omega)} + \frac{1}{(\omega_0 - i\gamma - 2\omega)(\omega_0 - i\gamma - \omega)} + \frac{1}{(\omega_0 + i\gamma + \omega)(\omega_0 - i\gamma - \omega)} \right\} \quad (4)$$

Ref. [23] has shown that Equation (4) can be written analogously to the Oudar-Chemla TLM:

$$\beta = \frac{3\Delta\mu \cdot |\mu_{ge}|^2}{\hbar^2} \frac{(\omega_0 - i\gamma)^2}{[(\omega_0 - i\gamma)^2 - \omega^2][(\omega_0 - i\gamma)^2 - 4\omega^2]} \quad (5)$$

This model is generally taken to describe homogeneously broadened media, which is clearly not descriptive of a complex molecule in liquid solution. Nonetheless, we will compare this with other models below to show that under certain circumstances, it yields a reasonable approximation.

Wang<sup>29</sup> has pointed out the inadequacy of Equation (5) in describing the dispersion of  $\beta$  near the two-photon resonance. The vibronic structure as the broadening mechanism was introduced to better describe the dispersion. In order to describe the dispersion in this way, the vibrational modes must be known in detail by, for instance, using computational modeling of the experimental absorption spectrum and resonance Raman excitation profiles.<sup>30-32</sup> In order to avoid the resonance Raman experiments and computational modeling, Kelly<sup>33</sup> has developed a semi-empirical approach using a direct mathematical transformation of the linear absorption band shape to obtain the hyper-Rayleigh dispersion, essentially a Kramers-Kronig transform relating the absorption coefficient to the index of refraction. In this case, Kelly finds:

$$\beta(-2\omega, \omega, \omega) = \frac{\Delta\mu}{2\pi c \hbar^2 (\omega_e - \omega)} \times \left[ \frac{\mu_{ge}^2 (2\omega_e + \omega)}{2\pi c (\omega_e + \omega)(\omega_e + 2\omega)} + \chi(2\omega) \right] \quad (6)$$

Here Kelly has used  $\omega_e$  as the average electronic transition frequency (averaged over the vibronic states, which we take as identical to  $\omega_0$ ). The term  $\chi(2\omega)$  is the linear susceptibility near the two-photon resonance. It is determined empirically as the imaginary part is obtained from the linear absorption spectra, and the real part from the Kramers-Kronig transform of the imaginary part. It should be noted that terms in the energy denominator containing positive frequencies have been omitted since they do not resonate at the frequencies in this experiment.

These two dispersion approaches will be used in the analysis of our data. Kelly's model will allow us to obtain accurate values for  $\Delta\mu$ . The CDHO model will provide a reasonably accurate analytical description for evaluation of Equation (3) since Kelly's model cannot be used to evaluate Equation (3) as it is semiempirical, and, therefore, not analytical.

## Experimental

The samples of di-8-ANEPPS used in our study were both purchased from Invitrogen, and synthesized by a procedure described by Loew and coworkers. The synthesis started with the Bucherer reaction of 6-bromo-2-naphthol to give 2-amino-6-bromonaphthalene. This aminonaphthalene was next reacted with 1-bromooctane to afford the dialkylated 2-(N,N-dioctyl)-6-bromonaphthalene which was coupled to 4-vinylpyridine using the palladium mediated Heck reaction. The resulting pyridine functionalized product was alkylated on nitrogen with 1,3-propane sultone to give the di-8-ANEPPS.

Figure (2) depicts the HRS experiment setup. A Q-switched Nd:YAG laser (Surelite II, Continuum) with a repetition rate of 10Hz and 7-ns pulse was used. The

1064nm laser output was followed by a frequency doubler and tripler to produce 355nm light, which was used to pump an OPO to obtain a variable wavelength output. The laser light passes through an analyzer and a Berek compensator set to  $\lambda/2$  retardation for the fundamental wavelength. The compensator is mounted on a computer-controlled rotation stage in order to adjust the polarization and intensity of the fundamental light. A small fraction of the incident fundamental light is focused onto a quartz plate for monitoring the fluctuations of the fundamental laser light so as to eliminate the shot-to-shot noise from the signal. (Reference channel) The fundamental light is focused into the sample solution in a square quartz cuvette (10x10 mm). The focal length is about 5cm, with the HRS signal collected at 90 degrees. In order to efficiently collect the second-order scattered light, a large aperture aspherical condenser is used (focal length is 2.5cm). The collimated light passes through a polarizer followed by a plano convex lens to focus the light into a photomultiplier tube. (Signal channel) Depending on which second harmonic wavelength is measured, a suitable color filter and an interference notch filter (10nm bandwidth) are used to block the fundamental light. The polarizer in front of the detector is added to measure the depolarization ratio of the Hyper-Rayleigh scattering in order to check the dimensionality of the molecule. The depolarization ratios we measured are  $0.28 \pm 0.05$  for pNA and  $0.24 \pm 0.03$  for di-8-ANEPPS which agree with the expected value of a one-dimensional molecule<sup>34, 35</sup>. Hyper-Rayleigh scattering measurements were carried out at five wavelengths: 800nm, 900nm, 976nm, 1020nm, and 1064nm. It was difficult to use wavelengths beyond this range because of the competing signal from background fluorescence. Appropriate wavelengths for measurement were determined from the collected emission spectra that showed little competing fluorescent emission.

In order to determine the hyperpolarizability  $\beta$  as a function of solvent polarity, two solvents of different polarity, dimethyl sulfoxide (DMSO) and chloroform, were mixed in various ratios. We found the two solvents to be completely miscible. The di-8-ANEPPS was first dissolved in a stock solution of DMSO at a concentration of 0.1mg/ml and then diluted to 0.02mg/ml into five solutions: A: pure DMSO solvent; B: 80% DMSO and 20% Chloroform; C: 60% DMSO and 40% Chloroform; D: 40% DMSO and 60% Chloroform; E: 20% DMSO and 80% Chloroform. Based on the refractive index and dielectric constant data of DMSO and chloroform, these solutions form a series of solutions of controlled polarity, as shown in Table 1. The dielectric constants and refractive indices of mixtures in the table were calculated by assuming linear scaling by fraction.

The emission spectra from the hyper-Rayleigh scattering experiments were initially collected using a spectrometer outfitted with an intensified CCD camera detector to verify in all cases (wavelengths and solvents) that the second harmonic signal was well separated from any fluorescence emission. Following this, hyper-Rayleigh scattering was measured at the appropriate polarization using photomultiplier tubes.

Para-nitroaniline (pNA) in acetone has been used as an external reference. Its hyperpolarizability value at 1064nm is  $24.5 \times 10^{-30} \text{ esu}^{36}$  and the Oudar-Chemla TLM was used to extrapolate the  $\beta$  values at other wavelengths. This extrapolation is reasonable because all of the wavelengths were far from the two-photon resonance where dispersion must be more carefully considered.

## Results and discussion

Figure 3 shows the linear absorption spectra of the Di-8-ANEPPS in DMSO and mixtures of DMSO and chloroform solvents. We can see the absorption spectrum shifts towards the blue at higher polarity (higher DMSO content), which agrees with the spectroscopic observation of similar dyes by Fromherz<sup>37</sup>.

From the linear absorption spectra,  $\omega_0$ ,  $\mu_{ge}$ , and  $\gamma$  can be calculated for each solvent and are plotted as a function of solvent polarity F in Figure (4). The electronic transition frequency  $\omega_0$  can be obtained from absorption peak. The transition moment  $\mu_{ge}$  can be calculated from the integrated molar absorptivity as:<sup>38</sup>

$$|\mu_{ge}|^2 = 9.185 \times 10^{-3} n \int \frac{\varepsilon[\varpi]}{\varpi} d\varpi \quad (7)$$

where n is the index of refraction,  $\varepsilon$  is the molar absorptivity in liters per mole per centimeter,  $\varpi$  is the wavenumber in inverse centimeters and the transition moment is in Debye. The  $\gamma$  is taken as the half-width at half maximum of the spectral transition, which can be obtained from fitting of the absorption spectra, as explained later. A linear fit is

used to obtain  $\frac{d\omega_0}{dF}$ ,  $\frac{d\mu_{ge}}{dF}$  and  $\frac{d\gamma}{dF}$ . We also plot  $\frac{d|\beta|}{dF}$  from hyper-Rayleigh scattering

data for all wavelengths. Figure (4) shows the four plots and linear fits. The fits yield

$\frac{d\omega_0}{dF} = 36500 \pm 7700$ ,  $\frac{d\mu_{eg}}{dF} = -16.9 \pm 2.1$  and  $\frac{d\gamma}{dF} = 5850 \pm 810$ . These results and a

model for the dispersion of  $\beta$  allow determination of the last three terms on the right-hand

side of Equation (3). We also determine the relative sensitivity  $\frac{1}{|\beta|} \frac{d|\beta|}{dF}$  values for the

wavelengths 800nm, 900nm, 976nm, 1020nm, and 1064nm (respectively:  $-5.9 \pm 3.1$ ,

$-4.5 \pm 4.0$ ,  $-9.0 \pm 3.8$ ,  $-13.8 \pm 4.3$  and  $-16.5 \pm 5.0$ ). These values will provide the data for the left-hand side of Equation (3).

In order to determine the first term on the right-hand side of Equation (3) involving  $\Delta\mu$ , we need to determine  $\Delta\mu$  from the hyper-Rayleigh scattering data. To do this, we plot the values of  $|\beta|$  at various wavelengths as shown in Figure (5). The quantity  $\Delta\mu$  is determined by fitting the data in Figure (5) to an appropriate model for the dispersion of  $\beta$ . We will fit to  $|\beta|$  as obtained by calculating the complex magnitude of both Equations (5) and (6) using  $\Delta\mu$  as an adjustable parameter. The other factors in Equations (5) and (6) are fixed as determined from the linear absorption data.

We show the fit to the absorption spectrum in pure DMSO as an example in Figure (6) to both a standard Lorentzian shape and also to a log-normal function<sup>39</sup>. We see that the log-normal function appears to be a better fit. However, we have determined  $\Delta\mu$  from both models. In order to obtain values of  $\omega_0$ ,  $\mu_{ge}$  and  $\gamma$  for calculating  $\Delta\mu$  from Equation (5), we need to fit the absorption  $\varepsilon(\omega)$  to a standard Lorentzian shape,<sup>40</sup>

$$\varepsilon(\omega) = A \frac{2\gamma}{(\omega - \omega_0)^2 + \gamma^2} \quad (8)$$

where  $\gamma$  is the HWHM of the spectral transition,  $A$  a scaling parameter and  $\omega_0$  is the transition frequency. The transition moment  $\mu_{ge}$  is calculated from Equation (7). Based on this Lorentzian fit to the linear absorption spectrum, we use mean values of  $\omega_0$ ,  $\mu_{ge}$  and  $\gamma$  as  $20048\text{cm}^{-1}$ ,  $10.7\text{D}$ ,  $2114\text{cm}^{-1}$  as the fixed parameters of the fit to  $\beta$  in Figure (5), using the CDHO model of Equation (5), we obtain  $\Delta\mu$  of  $20.2\text{ D}$ .

In order to calculate  $\Delta\mu$  from Equation (6), we employ the fit of the absorption data to the log-normal function,<sup>39</sup>

$$\varepsilon(\omega) = \frac{\varepsilon_0 b}{\omega - a} \exp(-c^2) \exp\left\{-\frac{1}{2c^2} \left[\ln\left(\frac{\omega - a}{b}\right)\right]^2\right\} \text{ for } \omega > a \quad (9)$$

and

$$\varepsilon(\omega) = 0 \text{ for } \omega \leq a \quad (10)$$

where the parameters  $a$ ,  $b$ ,  $c$  are related to resonant frequency  $\omega_0$  and HWHM of the spectral transition  $\gamma$  by

$$\omega_0 = a + b \exp(-c^2) \quad (11)$$

and

$$\gamma = b \exp(-c^2) \frac{\{\exp[2c(2 \ln 2)^{1/2}] - 1\}}{2 \exp[c(2 \ln 2)^{1/2}]} \quad (12)$$

We calculate the imaginary part of the linear susceptibility  $\chi(2\omega)$

from  $\sigma_a(\omega) = \frac{4\pi\omega}{3\hbar c n} \text{Im}[x(\omega)]$ . The real part of  $\chi(2\omega)$  needed to evaluate Equation (6) can

be obtained using the Kramers-Kronig relationship:<sup>41</sup>  $\text{Re}[\chi(\omega)] = \frac{2}{\pi} P \int_0^\infty \frac{\omega' \text{Im}[\chi(\omega')]}{\omega'^2 - \omega^2} d\omega'$ .

Using all of this in Equation (6), we find  $\Delta\mu$  of 13.0 D. We believe that this value for  $\Delta\mu$  is more accurate than that obtained from the CDHO model both heuristically, and because of its agreement with previous results,<sup>11</sup> which listed an estimated  $\Delta\mu$  of 14D. Note that it is likely that the  $\Delta\mu$  and  $\beta$  for this dye are negative which cannot be determined by hyper-Rayleigh scattering.<sup>42</sup> However, Equation (3) is insensitive to whether or not  $\Delta\mu$  is negative. We carried out this procedure for all of the values of F

from various solvent mixtures, with the results plotted in Figure (7). We note that we found similar slopes in both models, but the more accurate value of  $\Delta\mu$  from Equation (6).

Having all of the factors in the right-hand side of Equation (3) of the form of  $\frac{\partial}{\partial F}$ , we now must use an analytical expression for  $|\beta|$  to obtain the other factors. Kelly's semiempirical Equation (6) is not appropriate since there is no convenient and accurate analytical expression for the real part of  $\chi(2\omega)$ . Therefore, we must use the CDHO model. We note that the fits of Figure (5) do not clearly differentiate between the shapes of the model (although the  $\Delta\mu$  for the best fit is better for Kelly's model). We will apply the CDHO model, since it is analytic, and find that it is reasonable to do so.

Rewriting Equation (3) for the CDHO model of Equation (5), we obtain,

$$\frac{1}{|\beta|} \frac{d|\beta|}{dF} = \frac{1}{\Delta\bar{\mu}} \frac{\partial\Delta\mu}{\partial F} + \frac{2}{\bar{\mu}_{ge}} \frac{\partial\mu_{ge}}{\partial F} + A_{\bar{\omega}_0, \bar{\gamma}} \frac{\partial\omega_0}{\partial F} + B_{\bar{\omega}_0, \bar{\gamma}} \frac{\partial\gamma}{\partial F} \quad (13)$$

where A and B are given in the Appendix. The bars denote that the average values of the quantities (averaged over the various values corresponding to different F) are used in the calculation. In Figure (8) the data points indicate the sensitivity of the second harmonic intensity to a field as given by the left-hand side of Equation (13) and the results depicted in Figure (4d). The curve in Figure (8) is obtained by evaluating the right-hand side of Equation (13) and the results depicted in Figures (4a-c) and (7). We see that the data and model agree without adjustable parameters. We conclude that CDHO model given in Equation (13) is a reasonable description of the sensitivity of the second harmonic signal to local field. The imperfect fit is likely due to inadequacies of the CDHO description and the use of a two-level model, in general.

It is interesting to ask how each term in Equation (13) contributes to the overall sensitivity. Figure (9) depicts the contribution of each term to the sensitivity. First, it is clear that the contribution of the broadening  $\gamma$  is small, except perhaps near the resonance. This might explain why the CDHO model yields reasonable results despite its obvious shortcomings. Pons and Mertz<sup>16</sup> concluded that the highest sensitivity is obtained at the low energy side of resonance by only considering the Stark shift (third term on the right-hand side of Equation (13)). We concur with this conclusion, but find that the other contributions make this all the more dramatic. When considering the other contributions that are constant in frequency, the sensitivity on the high-energy side is minimal. It is clear that changes in the dipole moments with local field make significant contributions to the sensitivity as also seen in Figure (9). We also note that our analysis agrees well with trends of the sensitivities of similar dyes in biological imaging experiments<sup>17, 19</sup>, given the difference in the absorption spectra between our solutions and the biological environments. From the curve trend, at the fundamental wavenumber  $\sim 9000 \text{ cm}^{-1}$  (or at wavelength  $1.1 \mu\text{m}$ ), the relative sensitivity is maximal. We note that to the extent that the two-level model of the imaginary part of the second hyperpolarizability describes the sensitivity of the two-photon excited fluorescence (TPEF) response<sup>13</sup>, our results and conclusions can be applied to that imaging modality. We note, however, that, in the mode of two-color fluorescence ratio potentiometric imaging<sup>2</sup>, our model will not necessarily apply, as this modality implies that the frequency shift will dominate and frequency independent factors will not contribute.

Finally, we can make some remarks concerning solvatochromism. In the introduction, we indicated that the local field is closely related to the local electric field as

the relationship between solvatochromism and electrochromism. This relationship is model dependent, and will involve the Onsager reaction field, for example and phenomenological cavity radius parameter.<sup>43</sup> Thus, it is difficult to absolutely set the sensitivity scale in terms of the local field or membrane potential in Figure (8).

Our method suggests an assay for estimating the electronic sensitivity using only linear spectra. In this work, we utilized hyper-Rayleigh scattering to determine  $\Delta\mu$ . However,  $\Delta\mu$  can be estimated using solvent shifts for both linear absorption and emission where model dependent parameters, such as the cavity radius, are made to cancel. The excited state dipole moment of a quasi-one-dimensional dye can be determined through,<sup>21</sup>

$$\mu_e = \mu_g \frac{\Delta E_{emission}}{\Delta E_{absorption}} \quad (14)$$

where the ground state dipole moment must be independently known. With these measurements, the right hand side of Equation (3) can be estimated using only linear optical techniques.

## Conclusions

We have studied the electric field dependence for second harmonic generation in a potentiometric dye used in biological imaging using solvatochromic studies of hyper-Rayleigh scattering and linear absorption. Through a simple model relating the sensitivity of second harmonic generation to solvatochromic data of linear absorption, we can understand the contributions to the second harmonic sensitivity. We find that, in addition to the Stark shifts, that changes in dipole moments with local field, make significant contributions. We find that the dispersion of the sensitivity indicates that the

most sensitive wavelength for measurements is one half width lower in energy than the absorption peak, and the least sensitive is one half width higher in energy than the absorption peak. Our model and the use of solvatochromic linear absorption studies provides a reasonable assay for assessing the potential sensitivity of new chromophores with the proviso that additional measurements are needed to estimate the magnitude of the  $\Delta\mu$  term, which is important. We believe that our study has more general applicability, but further work is necessary to establish this.

## Acknowledgements

The authors are grateful for helpful discussions with Prof. Rolfe Petschek and Greg Wiggers. The authors acknowledge funding from the Ohio Board of Regents and the National Science Foundation under grant number DMR-0308730.

## Appendix

Here we calculate the partial derivatives of  $|\beta|$  with respect to  $\omega_0$  and  $\gamma$ . From

Equation (5)  $\beta = \frac{3\Delta\mu \cdot |\mu_{ge}|^2}{\hbar^2} \frac{(\omega_0 - i\gamma)^2}{[(\omega_0 - i\gamma)^2 - \omega^2][(\omega_0 - i\gamma)^2 - 4\omega^2]}$ , we obtain:

$$|\beta| = \frac{3\Delta\mu \cdot |\mu_{ge}|^2 (\gamma^2 + \omega_0^2)}{\hbar^2} \times$$

$$((\gamma^4 + 5\gamma^2\omega^2 + 4\omega^4)^2 + 2(2\gamma^6 + 5\gamma^4\omega^2 + \gamma^2\omega^4 - 20\omega^6)\omega_0^2$$

$$+ (6\gamma^4 - 10\gamma^2\omega^2 + 33\omega^4)\omega_0^4 + 2(2\gamma^2 - 5\omega^2)\omega_0^6 + \omega_0^8)^{-0.5}$$

We also calculate  $A = \frac{1}{|\beta|} \frac{\partial |\beta|}{\partial \omega_0}$  and  $B = \frac{1}{|\beta|} \frac{\partial |\beta|}{\partial \gamma}$  explicitly:

$$A = -[2\omega_0(\gamma^8 - 5\gamma^6\omega^2 - 32\gamma^4\omega^4 - 60\gamma^2\omega^6 - 16\omega^8 + (4\gamma^6 - 15\gamma^4\omega^2 + 32\gamma^2\omega^4 + 20\omega^6)\omega_0^2$$

$$\begin{aligned}
& +3(2\gamma^4 - 5\gamma^2\omega^2)\omega_0^4 + (4\gamma^2 - 5\omega^2)\omega_0^6 + \omega_0^8]/[(\gamma^2 + \omega_0^2)(\gamma^4 + 5\gamma^2\omega^2 + 4\omega^4)^2 \\
& +2(2\gamma^6 + 5\gamma^4\omega^2 + \gamma^2\omega^4 - 20\omega^6)\omega_0^2 + (6\gamma^4 - 10\gamma^2\omega^2 + 33\omega^4)\omega_0^4 + 2(2\gamma^2 - 5\omega^2)\omega_0^6 + \omega_0^8)] \\
B = & -[2\gamma(\gamma^8 + 5\gamma^6\omega^2 - 20\gamma^2\omega^6 - 16\omega^8 + (4\gamma^6 + 15\gamma^4\omega^2 + 32\gamma^2\omega^4 + 60\omega^6)\omega_0^2 \\
& + (6\gamma^4 + 15\gamma^2\omega^2 - 32\omega^4)\omega_0^4 + (4\gamma^2 + 5\omega^2)\omega_0^6 + \omega_0^8)]/[(\gamma^2 + \omega_0^2)(\gamma^4 + 5\gamma^2\omega^2 + 4\omega^4)^2 \\
& +2(2\gamma^6 + 5\gamma^4\omega^2 + \gamma^2\omega^4 - 20\omega^6)\omega_0^2 + (6\gamma^4 - 10\gamma^2\omega^2 + 33\omega^4)\omega_0^4 + 2(2\gamma^2 - 5\omega^2)\omega_0^6 + \omega_0^8)]
\end{aligned}$$

The  $A_{\bar{\omega}_0, \bar{\gamma}}$ ,  $B_{\bar{\omega}_0, \bar{\gamma}}$  values from Equation (13) are obtained by substituting the average values of  $\omega_0$ ,  $\gamma$  for the different polarity solvent mixtures.

## References

1. R. S. Bedlack, M. D. Wei, and L. M. Loew, "Localized Membrane Depolarizations And Localized Calcium Influx During Electric Field-Guided Neurite Growth," *Neuron* **9**(3), 393-403 (1992).
2. L. M. Loew, "Potentiometric dyes: Imaging electrical activity of cell membranes," *Pure And Appl. Chem.* **68**(7), 1405-1409 (1996).
3. E. Fluhler, V. G. Burnham, and L. M. Loew, "Spectra, Membrane-Binding, And Potentiometric Responses Of New Charge Shift Probes," *Biochem.* **24**(21), 5749-5755 (1985).
4. R. S. Ries, H. Choi, R. Blunck, F. Bezanilla, and J. R. Heath, "Black lipid membranes: visualizing the structure, dynamics, and substrate dependence of membranes," *J. Phys. Chem. B* **108**(41), 16040-16049 (2004).

5. T. Pons, L. Moreaux, O. Mongin, M. Blanchard-Desce, and J. Mertz, "Mechanisms of membrane potential sensing with second-harmonic generation microscopy," *J. Biomed. Opt.* **8**(3), 428-431 (2003).
6. L. Moreaux, T. Pons, V. Dambrin, M. Blanchard-Desce, and J. Mertz, "Electro-optic response of second-harmonic generation membrane potential sensors," *Opt. Lett.* **28**(8), 625-627 (2003).
7. L. Moreaux, O. Sandre, and J. Mertz, "Membrane imaging by second-harmonic generation microscopy," *J. Opt. Soc. Am. B* **17**(10), 1685-1694 (2000).
8. O. Bouevitch, A. Lewis, I. Pinevsky, J. P. Wuskell, and L. M. Loew, "Probing Membrane-Potential With Nonlinear Optics," *Biophys. J.* **65**(2), 672-679 (1993).
9. L. M. Loew, L. B. Cohen, B. M. Salzberg, A. L. Obaid, and F. Bezanilla, "Charge-Shift Probes Of Membrane-Potential - Characterization Of Aminostyrylpyridinium Dyes On The Squid Giant-Axon," *Biophys. J.* **47**(1), 71-77 (1985).
10. L. M. Loew and L. L. Simpson, "Charge-Shift Probes Of Membrane-Potential - A Probable Electrochromic Mechanism For Para-Aminostyrylpyridinium Probes On A Hemispherical Lipid Bilayer," *Biophys. J.* **34**(3), 353-365 (1981).
11. L. M. Loew, G. W. Bonneville, and J. Surow, "Charge shift optical probes of membrane potential. Theory," *Biochem.* **17**, 4065 (1978).

12. L. Sacconi, D. A. Dombeck, and W. W. Webb, "Overcoming photodamage in second-harmonic generation microscopy: Real-time optical recording of neuronal action potentials," *Proc. Nat. Acad. Sci.* **103**(9), 3124-3129 (2006).
13. M. Nuriya, J. Jiang, B. Nemet, K. B. Eisenthal, and R. Yuste, "Imaging membrane potential in dendritic spines," *Proc. Nat. Acad. Sci.* **103**(3), 786-790 (2006).
14. D. A. Dombeck, L. Sacconi, M. Blanchard-Desce, and W. W. Webb, "Optical recording of fast neuronal membrane potential transients in acute mammalian brain slices by second-harmonic generation microscopy," *J. Neurophys.* **94**(5), 3628-3636 (2005).
15. P. J. Campagnola, M. D. Wei, A. Lewis, and L. M. Loew, "High-resolution nonlinear optical imaging of live cells by second harmonic generation," *Biophys. J.* **77**(6), 3341-3349 (1999).
16. T. Pons and J. Mertz, "Membrane potential detection with second-harmonic generation and two-photon excited fluorescence: A theoretical comparison," *Opt. Commun.* **258**(2), 203-209 (2006).
17. A. C. Millard, L. Jin, J. P. Wuskell, D. M. Boudreau, A. Lewis, and L. M. Loew, "Wavelength- and time-dependence of potentiometric non-linear optical signals from styryl dyes," *J. Membrane Bio.* **208**(2), 103-111 (2005).
18. J. A. N. Fisher, B. M. Salzberg, and A. G. Yodh, "Near infrared two-photon excitation cross-sections of voltage-sensitive dyes," *J. Neuroscience Meth.* **148**(1), 94-102 (2005).

19. A. C. Millard, L. Jin, M. D. Wei, J. P. Wuskell, A. Lewis, and L. M. Loew, "Sensitivity of second harmonic generation from styryl dyes to transmembrane potential," *Biophys. J.* **86**(2), 1169-1176 (2004).
20. B. Kuhn, P. Fromherz, and W. Denk, "High sensitivity of stark-shift voltage-sensing dyes by one- or two-photon excitation near the red spectral edge," *Biophys. J.* **87**(1), 631-639 (2004).
21. P. Suppan and N. Ghoneim, *Solvatochromism* (Cambridge, Royal Society of Chemistry, 1997).
22. K. Clays and A. Persoons, "Hyper-Rayleigh Scattering In Solution," *Rev. Sci. Instr.* **63**(6), 3285-3289 (1992).
23. K. Clays and A. Persoons, "Hyper-Rayleigh Scattering In Solution," *Phys. Rev. Lett.* **66**(23), 2980-2983 (1991).
24. J. Zyss, T. C. Van, C. Dhenaut, and I. Ledoux, "Harmonic Rayleigh-Scattering From Nonlinear Octupolar Molecular Media - The Case Of Crystal Violet," *Chem. Phys.* **177**(1), 281-296 (1993).
25. T. W. Chui and K. Y. Wong, "Study of hyper-Rayleigh scattering and two-photon absorption induced fluorescence from crystal violet," *J. Chem. Phys.* **109**(4), 1391-1396 (1998).
26. J. L. Oudar and D. S. Chemla, "Hyperpolarizabilities of the nitroanilines and their relations to the excited state dipole moment," *J. Chem. Phys.* **66**(6), 2664 (1977).

27. B. S. Brunschwig, S. Ehrenson, and N. Sutin, "Solvent Reorganization In Optical And Thermal Electron-Transfer Processes - Solvatochromism And Intramolecular Electron-Transfer Barriers In Spheroidal Molecules," *J. Phys. Chem.* **91**(18), 4714-4723 (1987).
28. G. Berkovic, G. Meshulam, and Z. Kotler, "Measurement and analysis of molecular hyperpolarizability in the two-photon resonance regime," *J. Chem. Phys.* **112**(9), 3997-4003 (2000).
29. C. H. Wang, "Effects of dephasing and vibronic structure on the first hyperpolarizability of strongly charge-transfer molecules," *J. Chem. Phys.* **112**(4), 1917-1924 (2000).
30. A. M. Moran, D. S. Egolf, M. Blanchard-Desce, and A. M. Kelley, "Vibronic effects on solvent dependent linear and nonlinear optical properties of push-pull chromophores: Julolidinemalononitrile," *J. Chem. Phys.* **116**(6), 2542-2555 (2002).
31. A. M. Moran, C. Delbecque, and A. M. Kelley, "Solvent effects on ground and excited electronic state structures of the push-pull chromophore julolidinyl-n-N,N'-diethylthiobarbituric acid," *J. Phys. Chem. A* **105**(45), 10208-10219 (2001).
32. A. M. Moran and A. M. Kelley, "Solvent effects on ground and excited electronic state structures of p-nitroaniline," *J. Chem. Phys.* **115**(2), 912-924 (2001).
33. A. M. Kelley, "Frequency-dependent first hyperpolarizabilities from linear absorption spectra," *J. Opt. Soc. Am. B* **19**(8), 1890-1900 (2002).

34. G. J. T. Heesink, A. G. T. Ruiter, N. F. Vanhulst, and B. Bolger, "Determination Of Hyperpolarizability Tensor Components By Depolarized Hyper Rayleigh-Scattering," *Phys. Rev. Lett.* **71**(7), 999-1002 (1993).
35. J. L. Bredas, F. Meyers, B. M. Pierce, and J. Zyss, "On The 2nd-Order Polarizability Of Conjugated Pi-Electron Molecules With Octupolar Symmetry - The Case Of Triaminotrinitrobenzene," *J. Am. Chem. Soc.* **114**(12), 4928-4929 (1992).
36. P. Kaatz and D. P. Shelton, "Polarized hyper-Rayleigh light scattering measurements of nonlinear optical chromophores," *J. Chem. Phys.* **105**(10), 3918-3929 (1996).
37. P. Fromherz, "Monopole Dipole Model For Symmetrical Solvatochromism Of Hemicyanine Dyes," *J. Phys. Chem.* **99**(18), 7188-7192 (1995).
38. M. Klessinger and J. Michl, *Excited States and Photochemistry of Organic Molecules* (VCH, New York, 1995).
39. D. B. Siano and D. E. Metzler, "Band shapes of the electronic spectra of complex molecules," *J. Chem. Phys.* **51**(5), 1856 (1969).
40. P. W. Milonni and J. H. Eberly, *Lasers* (J. Wiley and Sons, 1998).
41. A. Yariv, *Quantum Electronics, 2nd Edition* (Wiley, New York, 1975).
42. H. Li, "Nonlinear Optical Studies of Potential-Sensitive Dyes," Ph.D. Dissertation (Case Western Reserve University, Cleveland, 2007).

43. W. Liptay, "Electrochromism and Solvatochromism," *Angewand. Chem. Int. Ed.* **8**(3), 177-188 (1969).

## List of Figures

**Figure 1.** Structure of di-8-ANEPPS.

**Figure 2.** Experimental setup for HRS measurements as described in the text.

**Figure 3.** Linear absorption spectra of di-8-ANEPPS in solutions A, B, C, D and E.

Absorption spectrum shifts toward the red as the polarity decreases from A to E.

**Figure 4.** Solvent polarity ( $F$ ) dependent measured quantities. a) Absorption frequency, b) transition moment, c) spectral half-width and d) first hyperpolarizability. (Solid square 800nm, open square 900nm, triangle 976nm, solid circle 1020nm, and open circle 1064nm in d.)

**Figure 5.** Hyperpolarizability  $\beta$  of di-8-ANEPPS in DMSO solution (Dots),  $F = 0.220$ , and fit to Equations (5) Solid line and (6) Dashed line.

**Figure 6.** Linear absorption spectra of di-8-ANEPPS in DMSO solution (Solution A, solid line). Dashed line is the Log-normal fit for the first electronic absorption band. Dot-Dash is the CDHO lineshape fit.

**Figure 7.** Plot of  $\Delta\mu$  versus  $F$  and the corresponding linear fit.

**Figure 8.** Relative second harmonic sensitivity as a function of frequency. Solid line is the model of Equation (7) (right-hand side), and data is the left-hand side of Equation (7).

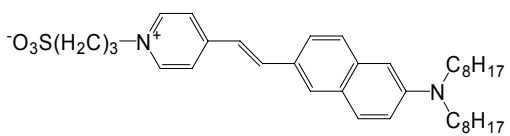
**Figure 9.** Contributions of different terms as a function of frequency. The solid line is the  $\omega_0$  term and the dashed line is the  $\gamma$  term, both of which are frequency dependent. The Dash-Dot line is the  $\mu_{eg}$  term and the Dot line is the  $\Delta\mu$  term, both of which are frequency independent.

Table 1. Solution properties.  $F$  is the polarity,  $\epsilon$  the dielectric constant, and  $n$  the refractive index. Data for mixtures are calculated from algebraic sum of the cosolvent fractions using  $\epsilon$  and  $n$  of chloroform as 4.81 and 1.4458, respectively<sup>a</sup>.

<b>Solution</b>	<b>F</b>	<b><math>\epsilon</math></b>	<b><math>n</math></b>
A (DMSO)	0.2195	46.68 <sup>a</sup>	1.4793 <sup>a</sup>
B	0.2176	38.31	1.4726
C	0.2139	29.93	1.4659
D	0.2064	21.56	1.4592
E	0.1883	13.18	1.4525

a: data from Burdick & Jackson website for corresponding HPLC solvent at 20 °C

**Figure 1.** Structure of di-8-ANEPPS.



**Figure 2.** Experimental setup for HRS measurements as described in the text.

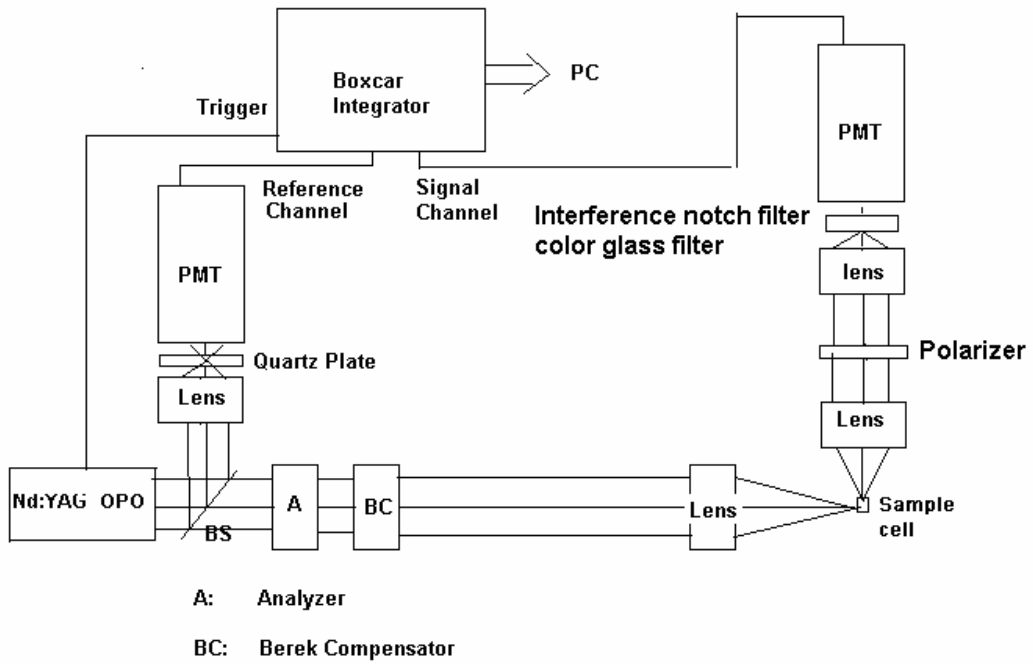


**Figure 3.** Linear absorption spectra of di-8-ANEPPS in solutions A, B, C, D and E.

Absorption spectrum shifts toward lower wavenumber as the polarity decreases from A (rightmost curve) to E (leftmost curve).

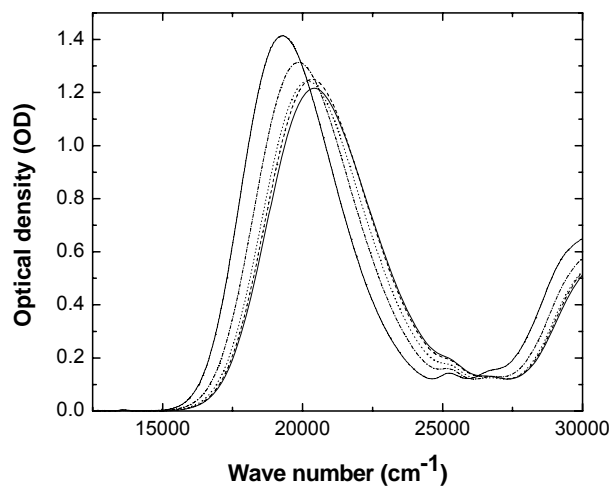


**Figure 4.** Solvent polarity ( $F$ ) dependent measured quantities. a) Absorption frequency, b) transition moment, c) spectral half-width and d) first hyperpolarizability. (Solid square 800nm, open square 900nm, triangle 976nm, solid circle 1020nm, and open circle 1064nm in d.)

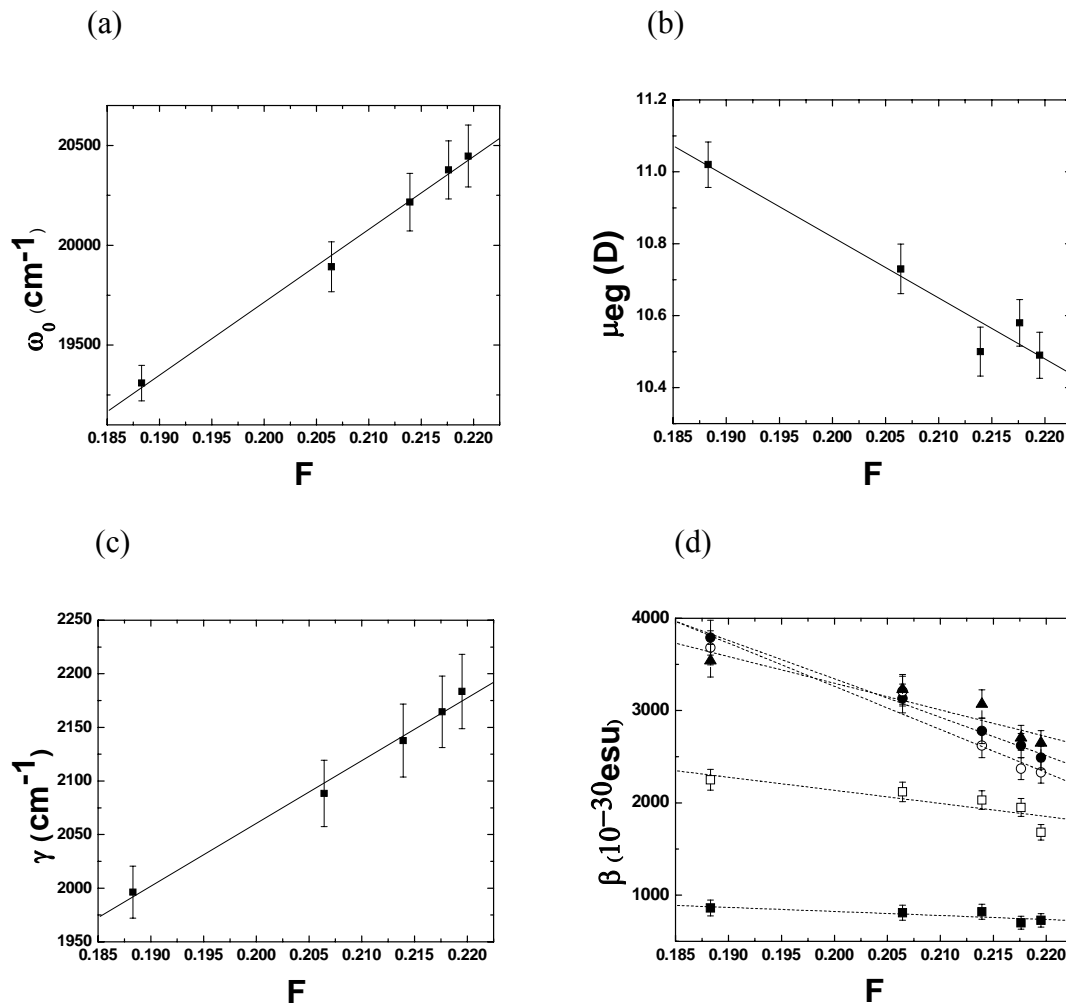


**Figure 5.** Hyperpolarizability  $\beta$  of di-8-ANEPPS in DMSO solution (Dots),  $F = 0.220$ , and fit to Equations (5) Solid line and (6) Dashed line.

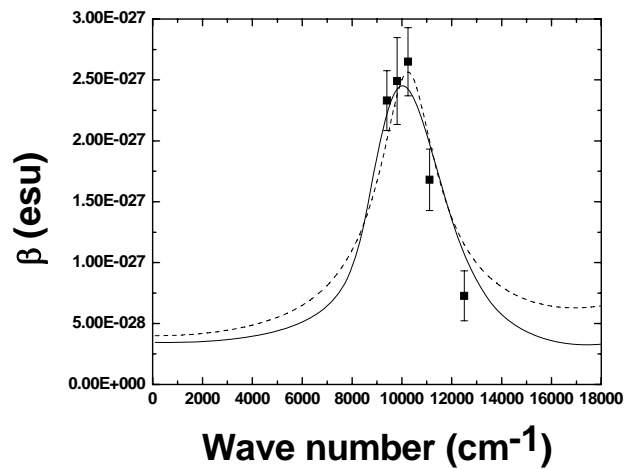


**Figure 6.** Linear absorption spectra of di-8-ANEPPS in DMSO solution (Solution A, solid line). Dashed line is the Log-normal fit for the first electronic absorption band. Dot-Dash is the CDHO lineshape fit.

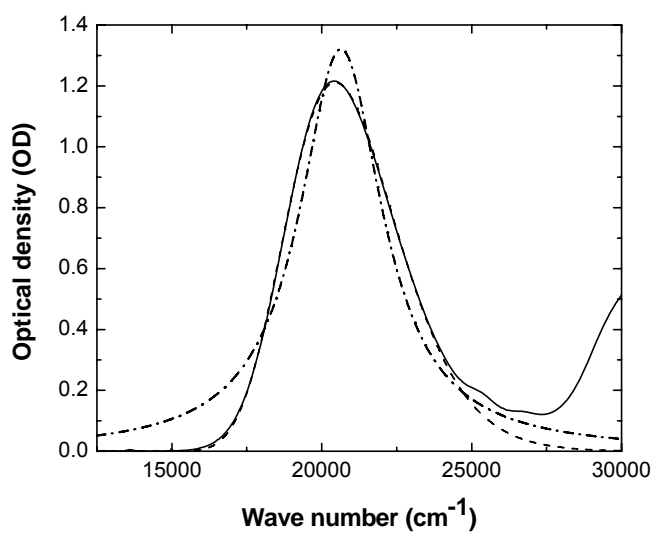


**Figure 7.** Plot of  $\Delta\mu$  versus  $F$  and the corresponding linear fit.

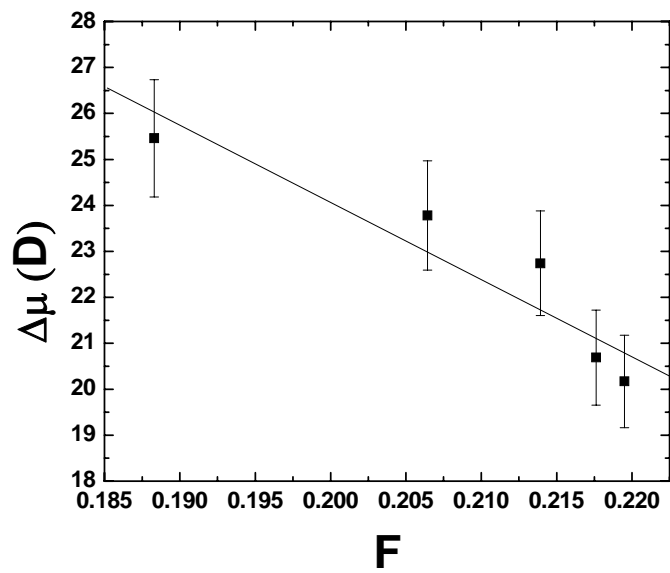


**Figure 8.** Relative second harmonic sensitivity as a function of frequency. Solid line is the model of Equation (13) (right-hand side), and data is the left-hand side of Equation (13).

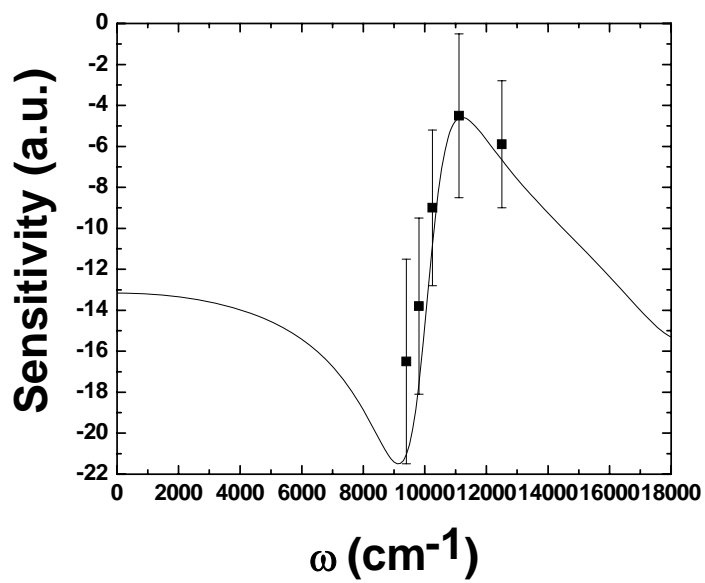


**Figure 9.** Contributions of different terms of Equation (3) as a function of frequency.

Labels indicate the variable of the partial derivative in that equation.

